

# Importance of Leakage Magnetic Field and Fringing Flux in Surge Protector Design

Sadeeshvara Silva Thotabaddadurage, *Member, IEEE*; Nihal Kularatna, *Senior Member, IEEE* and D. Alistair Steyn-Ross, *Senior Member, IEEE*

**Abstract**—Transient surge absorption capability of supercapacitors is practically implemented in a commercial surge protector known as supercapacitor assisted surge absorber (SCASA). It is a low component count high performance circuit design which utilizes a coupled inductor topology wound to a powdered-iron magnetic core. This paper investigates non-ideal characteristics of the SCASA transformer designed using various air-gapped ferrites such as manually gapped toroids and mass-produced commercially available EER cores. Emphasis is given to examine surge energy losses associated with leakage magnetic field and fringing flux of gapped transformer prototypes. In predicting effects of an air gap in ferrite materials, an analytical approach based on effective-permeance is used with validations based on SCASA inductance properties. Experimental work presented in this paper are carried out using a Noiseken lightning surge simulator adhering to IEC 60038 and IEEE C62.41 standards. In addition, SCASA prototypes were subjected to surge immunity tests specified by UL-1449 Underwriters’ laboratory procedures, where a 10% reduction of load-voltage was recorded outperforming the present design.

**Index Terms**—Magnetic leakage, Fringing flux, Effective-permeance, Surge Protection, SCASA, Supercapacitors

## I. INTRODUCTION

Modern semiconductor based electronic systems are vulnerable to various power quality issues such as AC mains fluctuations, transients, harmonics and noise; hence, the need for processing and conditioning of electrical power has emerged as an essential requirement [1]. Out of these power problems, transients caused by lightning or heavy inductive loads could reach peak amplitudes of several thousands of volts (> 900 V), creating the greatest voltage stress to sensitive load equipment causing circuit failures [2]. A well designed surge protector device (SPD) can prevent detrimental effects of a transient by absorbing and dissipating its energy to safeguard a load, while continually facilitating the mains electricity [3]. This paper presents design aspects of magnetic components of a patented SPD known as SCASA technique using different

air-gapped ferrite cores. Compared to the existing SCASA topology that shows satisfactory performance, this research elucidates optimization strategies to reduce load voltage by 10% based on high-performance prototypes developed using air-gapped ferrite toroids and gapped EER cores. While providing superior protection to the critical load, the new prototypes described in this paper improves surge endurance of the present design with a 40% reduction of the manufacturing cost. Next, fundamental principles of surge protection and details of SCASA magnetic core will be discussed.

## A. Fundamentals of Surge Protection

Based on the voltage division principle [4], a SPD protects the critical load by incorporating two fundamental compo-

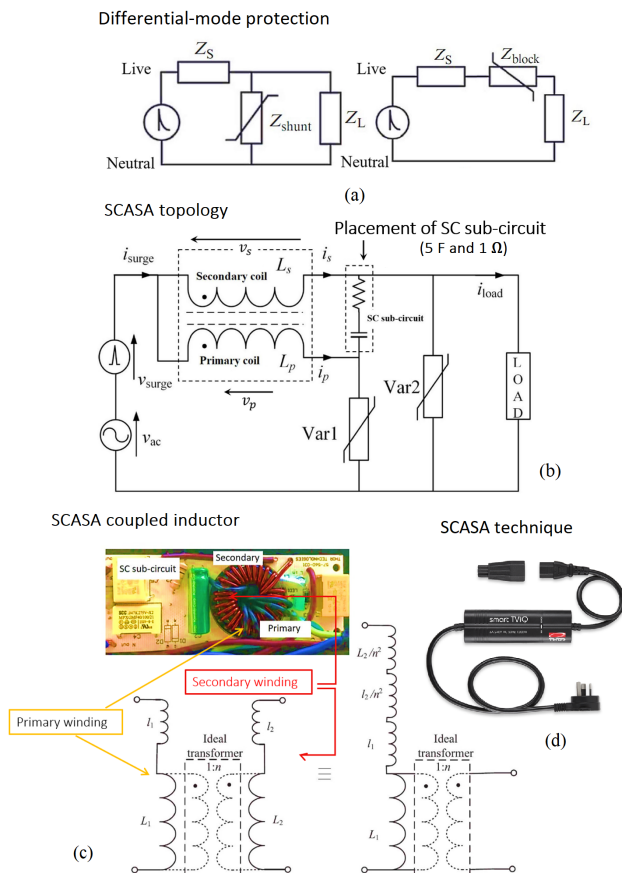


Fig. 1. Principles of differential-mode protection and SCASA design: (a) use of shunt and series surge-blocking elements; (b) SCASA circuit topology; (c) equivalent circuit of SCASA coupled-inductor core (d) commercial implementation of SCASA

Manuscript received Month xx, 2xxx; revised Month xx, xxxx; accepted Month x, xxxx.

Sadeeshvara Silva Thotabaddadurage, Nihal Kularatna and D. Alistair Steyn-Ross: School of Engineering, University of Waikato, Hamilton, 3240, New Zealand (email: nihalkul@waikato.ac.nz; asr@waikato.ac.nz).

Correspondence: Sadeeshvara Silva Thotabaddadurage, Electric Power Engineering Centre, University of Canterbury, Christchurch, 8140, New Zealand (email: sadeesh.silva@canterbury.ac.nz or sadeeshvara.udayanga@gmail.com).

ment types.  $Z_{\text{block}}$  type components such as inductors which generate large impedances ( $\omega L$ ) at high-frequency transients can attenuate and block the propagation of transient energy towards sensitive load as shown by Fig. 1(a). Comparably,  $Z_{\text{shunt}}$  components such as capacitors, metal oxide varistors (MOVs) and bidirectional break-over diodes (BBDs) show a reduced impedance ( $1/\omega C$  or reduced non-linear resistance for MOVs/BBDs) under high frequencies diverting the transient away from the load [2,5]. In both cases, the path impedance  $Z_s$  (due to loop resistances and stay-line inductances) provides an extra series protection against the surge. In developing SCASA, both  $Z_{\text{block}}$  and  $Z_{\text{shunt}}$  protection elements are being adopted as described below.

## B. Overview of SCASA Technique

SCASA technique was originally developed by the power electronics research group at the University of Waikato based on the surge withstanding capability of supercapacitors (SCs) [6]. The unique SCASA topology illustrated by Fig. 1(b) allows a SC to be placed inside a surge protector without exposing it to 230 V, thus the SC can safely operate without exceeding its low DC rating of 2.7–3 V [7]. Moreover, with the low component count, a commercial product based on SCASA design ("Smart TViQ") has been implemented by Thor Technologies, Australia [8].

1) *Design Configuration of SCASA Magnetic Core:* In designing SCASA, a coupled-inductor topology (as  $Z_{\text{block}}$ ) is adopted by utilizing a powdered-iron core (Kool  $\mu$  0077071A7- Magnetics Inc.) which has a relative permeability  $\mu_r = 60$  [9]. As per Fig. 1(b), the two coupled windings are configured in such way that the less inductive (3.4  $\mu$ H) primary coil with 6 turns ( $N_1$ ) provides a lower impedance path for surge propagation than the more inductive (57  $\mu$ H) secondary with 28 turns ( $N_2$ ). Thus, it was validated that  $\sim 90\%$  of transient current passes through primary coil firing Var1, whereas the opposing voltage barrier  $v_s$  induced in secondary prevents transient currents flowing into the load-side. Though a turns ratio of 4.67 is predicted according to the coupled configuration, it was experimentally found that the inverse current-ratio does not match with the turns-ratio due to non-ideal behaviour of the SCASA transformer. Combined magnetic action of the two coupled coils minimizes the transient stress on the load by storing surge energy within the SCASA toroid. Furthermore, two MOVs (Var1 and Var2) which act as  $Z_{\text{shunt}}$  protection elements dissipate most of transient energy as heat. More details about SCASA configuration can be found in [10, 17].

2) *Magnetics of SCASA Coupled Inductor:* In separate research [11, 21], a permeance based theoretical model was developed to predict non-ideal characteristics of the SCASA magnetic core. The primary and secondary coupled-inductor windings of SCASA transformer possess magnetizing inductances ( $L_1, L_2$ ) and leakage inductances ( $l_1, l_2$ ) as described by Fig. 1(c). As per the definitions of magnetizing permeance ( $\Lambda_m$ ) and leakage permeance ( $\Lambda_\sigma$ ) [12], self-inductances of both primary ( $L_p$ ) and secondary ( $L_s$ ) windings can be expressed as:

$$L_p = \Lambda_m N_1^2 + \Lambda_\sigma N_1^2 \quad (1)$$

$$L_s = \Lambda_m N_2^2 + \Lambda_\sigma N_2^2 \quad (2)$$

In theorizing both  $L_p$  and  $L_s$ , the permeance values  $\Lambda_m$  and  $\Lambda_\sigma$  can be extracted from the manufacturer specifications (Magnetics Inc.) of the particular Kool  $\mu$  0077071A7 toroid. Since this paper aims at investigating the optimization of present SCASA design based on air-gapped ferrites, the importance of gapping a magnetic core will be discussed in the next Section.

## II. THEORETICAL MODELS FOR AN AIR-GAPPED TOROID

In this section, use of air-gapped ferrite toroids for the present SCASA design is investigated, and methods to enhance the energy storage capacity of the coupled-inductor are explored in order to optimize circuit performance. Starting from the permeance based analytical approach described above, theoretical models for effective-permeability and effective-permeance of an air-gapped toroid are developed in this Section.

### A. Importance of an Air-gap in Ferrite-iron

A high permeability material such as ferrite-iron is one that has a low reluctance for a given magnetic path length (MPL) and core cross-section [13]. Specially soft ferrites (W and H ferrites) have relative permeabilities in the range 5000-15,000 [16]; thus, they can be magnetized and demagnetized easily, and their hysteresis core losses are small [12]. Moreover, ferrite materials are resistant to sustain magnetism; thus, have a very low magnetic energy storage capability due to their low core reluctance [12,13]. However, when a relative medium like air is introduced into a ferrite core, it will elevate the magnetic hardness of the core leading to a greater energy storage [14,15].

Moreover, when an air-gap is inserted to the magnetic path, the resulting media will have a sheared B-H loop leading to a significant reduction in core's permeability (Fig. 2) [13]. Under such conditions, an effective-permeability is defined for the toroid which in-cooperates two media (ferrite and air) present in the magnetic path [15]. Noticeably, the magnetizing force  $H$  required to reach saturation flux density ( $B_{\text{sat}}$ ) is much larger for an air-gapped core that would otherwise reach saturation at a low level under ungapped conditions (Fig. 2). Therefore, another essential attribute of the air gap in surge applications is to reduce possibilities of core saturation.

### B. Effective-Permeability of an Air-gapped Toroid

The alteration effect of core reluctance due to an air gap is described in [15]; based on the combined effect of ferrite and air in the magnetic path, the effective-permeability  $\mu_l'$  of an air-gapped toroid can be derived as,

$$\mu_l' = l_c \left[ \frac{\mu_r}{\mu_r l_g + l_c} \right] \quad (3)$$

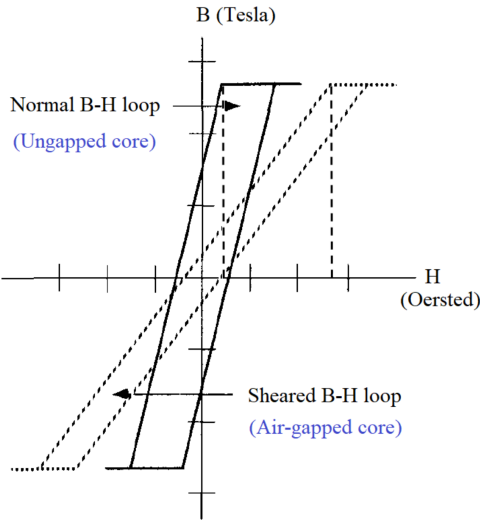


Fig. 2. The shearing of an idealized B-H loop due to an air gap: comparison between ungapped and air-gapped toroidal cores [13]

where  $l_c$  is circular length of the core,  $l_g$  is air-gap length,  $\mu_r$  is the relative permeability of an ungapped core.

This result confirms the reduction of permeability in the presence of a relative medium such as air. When:

$$l_g = 0 \rightarrow \mu_l' = \mu_r$$

$$l_g > 0 \rightarrow \mu_l' < \mu_r$$

For a single air-gapped toroid (Fig. 3) with a gap length  $l_g = 2$  mm,  $l_c = 100$  mm and  $\mu_r = 10,000$ , using (3):

$$\mu_l' = 100 \text{ mm} \left[ \frac{10,000}{10,000 \times 2 \text{ mm} + 100 \text{ mm}} \right]$$

$$\mu_l' \approx 50$$

This calculation justifies that insertion of an air gap to the ferrite provides a significant reduction in relative permeability (10,000  $\rightarrow$  50). Next, a formula for the effective-permeance of a gapped core is derived.

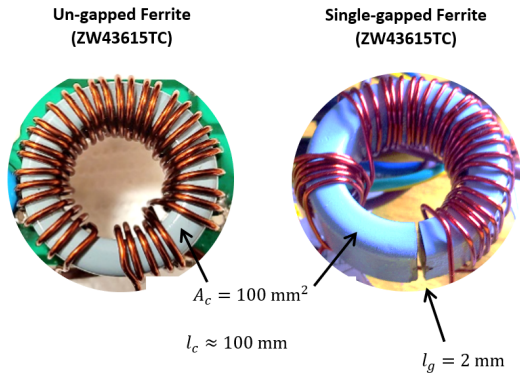


Fig. 3. Geometrical configurations of ungapped and single-gapped ferrite toroids

### C. Effective-Permeance of an Air-gapped Toroid

The reduction of core permeability increases the reluctance of equivalent magnetic circuit leading to a reduction in core permeance. Specially, due to the presence of two materials (ferrite metal and air) inside the toroid, a new relationship for the core's effective-permeance can be derived starting from the definition described in Section I-B2. As per (4), magnetizing permeance  $\Lambda_m$  of an ungapped ferrite core:

$$\Lambda_m = \frac{\mu_r \mu_0 A_c}{l_c} \quad (4)$$

Since  $\mu_r$  of an ungapped core changes to effective permeability  $\mu_l'$  in an air-gapped toroid, (3) and (4) can be combined to introduce an effective permeance  $\Lambda_m'$  for the core:

$$\Lambda_m' = \frac{l_c \left[ \frac{\mu_r}{\mu_r l_g + l_c} \right] \mu_0 A_c}{l_c} \quad (5)$$

(5) simplifies into:

$$\Lambda_m' = \frac{\mu_r \mu_0 A_c}{[\mu_r l_g + l_c]} = \frac{\mu_0 A_c}{[l_g + l_c/\mu_r]} \quad (6)$$

As  $\mu_r$  for a pure ferrite is significantly larger ( $\mu_r \gg 1$ ,  $\mu_r \sim 10,000$ ), it is clear that even the effective permeance ( $\Lambda_m'$ ) for an air-gapped toroid is substantially smaller than the magnetizing permeance ( $\Lambda_m$ ) of an ungapped toroid. Dividing (6) by (4) yields:

$$\frac{\Lambda_m'}{\Lambda_m} = \frac{1}{\left[ 1 + \frac{\mu_r l_g}{l_c} \right]} \quad (7)$$

For a single-gapped ferrite core as shown in Fig. 3, when  $l_g = 2$  mm,  $l_c = 100$  mm and  $\mu_r = 10,000$ :

$$\Lambda_m' \approx 0.005 \Lambda_m \quad (8)$$

$$\Lambda_m \gg \Lambda_m'$$

This result further confirms the reduction of magnetizing permeance in the presence of an air-gap. According to the manufacturer specifications [16] of W-ferrite toroid (ZW43615TC)  $\Lambda_m = 13,400$  nH/turn<sup>2</sup>; thus,  $\Lambda_m'$  for the single-gapped core can be calculated as:

$$\Lambda_m' = 0.005 \times 13,400 \text{ nH/turn}^2 \approx 67 \text{ nH/turn}^2$$

This effective-permeance of the gapped toroid matches well with the existing Kool  $\mu\mu$  (0077071A7) powdered-iron core of present SCASA design that has a permeance of 61 nH/turn<sup>2</sup>.

### D. Magnetic Energy Storage

As described previously, the main purpose of inserting an air-gap into the ferrite core is to enhance its energy storage capacity. Using Ampere's law, energy  $E_o$  stored in the air gap can be derived as below; details about this derivation is given in [17].

$$E_o = \frac{1}{2} \frac{B^2 v g}{\mu_0} \quad (9)$$

Here,  $\vec{B}$  is the magnetic flux density through the core and  $v_g$  is the volume of air-body as indicated by Fig. 3. This air volume can be easily found using  $A_c l_g$ . To compare the energy storage capability of ungapped and single-gapped ferrite toroids, a proportional relationship based on (9) is considered.

As surge related magnetic flux due to transient currents flows uniformly through the core and air-gap, energy  $E_c$  stored in the pure ferrite can be expressed as proportional to,

$$E_c \propto \frac{A_c l_c}{\mu_o \mu_r}$$

Similarly, energy stored in the air-column of single-gapped core is proportional to,

$$E_o \propto \frac{A_c l_g}{\mu_o}$$

Based on above relationships,  $E_o/E_c$  can be found as:

$$\frac{E_o}{E_c} = \frac{\mu_r l_g}{l_c}$$

For a single-gapped toroid with a gap length  $l_g = 2$  mm,  $l_c = 100$  mm and when  $\mu_r = 10,000$  for the pure ferrite core, using above relationship:

$$\frac{E_o}{E_c} = \frac{10,000 \times 2 \text{ mm}}{100 \text{ mm}}$$

$$E_o = 200 \times E_c$$

Notably, this proves that the magnetic energy stored in the air-gap itself is 200 times greater than the energy stored in entire core body of the ungapped toroid [17]. Next, the usability of mass produced commercial gapped ferrites will be investigated in designing SCASA prototypes.

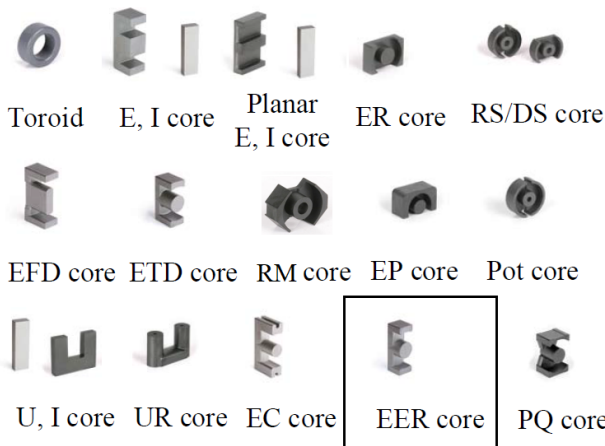


Fig. 4. Various ferrite core shapes from 2020 Magnetics Inc. ferrite-core catalogue [16]

### III. SCASA DESIGN USING COMMERCIAL GAPPED FERRITES

#### A. Selection of Core Geometry and Material

In Section II, the importance of air-gapped ferrites in optimizing the performance of SCASA was explained. But, the gapping approach used by externally cutting the toroid was a difficult task. Specially due to the brittleness of ferrite like material, there is a high possibility of fracture within the toroid during cutting process. Moreover, the feasibility of mass production using this gapping method is highly limited. Therefore, an initial investigation was carried out in selecting the best commercially available gapped-ferrites suitable for SCASA surge protector design. Fig. 4 illustrates various ferrite core geometries manufactured by Magnetics Inc., USA.

According to the manufacturer specifications, any geometrical configuration shown in Fig. 4 can be incorporated with an air-gap provided that the gap-code or the effective-permeance  $\Lambda'_m$  (also known as inductance factor  $A_L$  for a gapped core) is accurately specified. Given the suitability for SCASA topology and the overall cost in gapping (varies depending on the shape), EER type gapped core is selected for prototype construction. Consistent with the  $\Lambda_m$  of original Kool  $\mu$  powdered-iron toroid described in Section II-C,  $\Lambda'_m$  of this commercially available gapped EER core was determined as  $\sim 125$  nH/turn<sup>2</sup>. Notably, this standard off-the-shelf EER core indicated a significant cost reduction compared to the original Kool  $\mu$  powdered-iron toroid. More details about the cost comparison is presented at the end of this Section VI.

TABLE I  
COMPARISON OF MAGNETIC PROPERTIES OF UNGAPPED FERRITE MATERIALS MANUFACTURED BY MAGNETICS INC., USA [16]

MATERIAL		INDUCTORS & POWER TRANSFORMERS					EMI/RFI FILTERS & BROADBAND TRANSFORMERS		
		L	R	P	F	T	J	W	
Initial Permeability	$\mu_i$	900 ±25%	2,300 ±25%	2,500 ±25%	3,000 ±20%	3,000 ±25%	5,000 ±20%	10,000 ±30%	
Maximum Usable Frequency (50% roll-off)	f	/MHz	≤6	≤1.8	≤1.8	≤1.5	≤1.5	≤0.7	≤0.5
Relative Loss Factor X 10 <sup>4</sup> 25°C		tan δ/ $\mu_{oc}$						≤15 100 kHz	≤7 10 kHz
Curie Temperature	$T_c$	°C	>300	>210	>210	>210	>220	>145	>135
Flux Density @ 1,194 A/m (15 Oe) 25°C	$B_m$ 10 kHz	G mT	4,200 420	4,700 470	4,700 470	4,700 470	5,300 530	4,300 430	3,900 390

Another useful consideration that is relevant to the core selection is the material composition. Since ferrite based materials used in core manufacturing has a wide range including W, J, T, F, P and R ferrites, a detailed comparison about magnetic properties of each type was carried out. Table I presents a summary of essential magnetic parameters of different ferrite materials.

The above information presented in Table I is applicable to all pure ferrite materials without air-gaps. When a selected core geometry is manufactured incorporating gaps, these magnetic properties are altered accordingly. The material choice for SCASA was R-ferrite due to its relatively lower initial permeability ( $\mu_r = 2,300$ ) compared to extremely high permeability of W-ferrite ( $\mu_r = 10,000$ ). Hence, the air-gap to be inserted was not as wider as what was required

for W-ferrite toroid discussed in Section II. The effective-permeability required for SPD application can be achieved conveniently using R-ferrite with a thin-gap leading to a reduced manufacturing cost. Also, due to the high availability and greater saturation flux density of R-ferrite compared to W, J and L ferrites, R material selection (Table I) can be further justified. Materials like T-ferrites, though comparatively better in saturation level, are rare and expensive. Considering aforementioned factors, SCASA prototypes are constructed using a R-ferrite based gapped EER core (R43521A125). The gap code for the selection was A-125 meaning that the effective-permeance  $\Lambda'_m = 125 \text{ nH/turn}^2$  which is comparable to the original Kool  $\mu\text{U}$  powdered-iron core. Fig. 5 illustrates the R43521A125 core before and after the winding. More details about the effective-permeance and effective-permeability of gapped EER core are presented next.

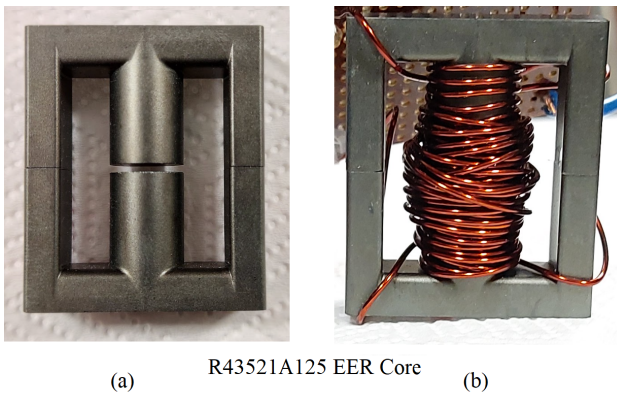


Fig. 5. R43521A125 air-gapped EER core: (a) unwound core; (b) wound core installed in SCASA surge protector

### B. Effective-permeability and Effective-Permeance of air-gapped EER core

Based on the gap code (A-125) of selected R43521A125 EER core [18], the effective-permeance  $\Lambda'_m$  is determined as  $125 \text{ nH/turn}^2$ . Compared to the permeance  $\Lambda_m$  of the original ungapped EER core, to examine the reduction of  $\Lambda'_m$  in the presence of an air-gap, a proportional relationship is considered as described below. Given  $\mu_r = 2,300$  for a R-ferrite material, the  $\Lambda_m$  of original EER core was found as  $2725 \text{ nH/turn}^2$  [18]. This is significant drop of  $\Lambda_m \rightarrow \Lambda'_m$  is quantified by the following calculations.

Permeance of the original ungapped EER core:

$$\Lambda_m = 2725 \text{ nH/turn}^2$$

Effective permeance of the air-gapped EER core:

$$\Lambda'_m = 125 \text{ nH/turn}^2$$

Thus, the ratio  $\Lambda_m:\Lambda'_m$  can be approximated as:

$$\frac{\Lambda_m}{\Lambda'_m} = \frac{2725 \text{ nH/turn}^2}{125 \text{ nH/turn}^2} \approx 22 \quad (10)$$

$$\Lambda'_m = 0.046 \times \Lambda_m$$

Eq. (10) proves the reduction of permeance into effective-permeance in the presence of an air-gap in EER core as shown by Fig. 5. Another useful result obtained from (10) is the prediction of effective permeability  $\mu'_r$  of gapped EER core. As per the definition of magnetizing permeance described in (4), for a given core geometry,  $\Lambda_m$  is proportional to  $\mu_r/l_c$ :

$$\Lambda_m \propto \frac{\mu_r}{l_c} \quad (11)$$

By analogy, for the air-gapped EER core:

$$\Lambda'_m \propto \frac{\mu'_r}{l_c + l_g} \quad (12)$$

Dividing (11) by (12), and by using (10) mentioned above:

$$\frac{\Lambda_m}{\Lambda'_m} = \frac{\mu_r \times [l_c + l_g]}{\mu'_r \times l_c} = \frac{2725 \text{ nH/turn}^2}{125 \text{ nH/turn}^2} \quad (13)$$

Since air-gap length  $l_g$  is much smaller compared to path length  $l_c$  of the core ( $l_g \ll l_c$ ), by approximating  $l_c + l_g \approx l_c$ , (13) simplifies into:

$$\frac{\Lambda_m}{\Lambda'_m} = \frac{\mu_r}{\mu'_r} = 22 \quad (14)$$

By rearranging (14), effective relative permeability  $\mu'_r$  of the gapped EER core shown in 5 can be obtained as:

$$\mu'_r = \frac{\mu_r}{22} = \frac{2,300}{22} \approx 105 \quad (15)$$

The mathematical relationship obtained above clearly indicates the significance of air-gap inside EER core which results in a substantial drop in magnetic permeability. Compared to pure R-ferrite material ( $\mu_r = 2,300$ ) described in Table I, this commercially available air-gapped EER core (R43521A125) yielded an effective-permeability  $\mu'_r = 105$ . Notably,  $\mu'_r$  lies in a comparable range with Kool  $\mu\text{U}$  powdered-iron core (0077071A7) which had  $\mu_r = 60$ . A comparison of relative permeability and permeance of the two core types is presented in Table II.

TABLE II  
COMPARISON OF RELATIVE PERMEABILITY AND PERMEANCE COEFFICIENTS OF KOOL  $\mu\text{U}$  POWDERED-IRON CORE (0077071A7), GAPPED AND UNGAPPED EER CORE (R43521A125/R43521) TYPES [17]

	Kool $\mu\text{U}$ Toroid (0077071A7)	Un-gapped EER core (R43521)	Air-gapped EER core (R43521A125)
Relative Permeability/ Effective Relative Permeability ( $\mu_r/\mu'_r$ )	$\mu_r = 60$	$\mu_r = 2300$	$\mu'_r = 105$
Permeance/Effective Permeance - $\Lambda_m/\Lambda'_m$ ( $\text{nH/turn}^2$ )	$\Lambda_m = 61$	$\Lambda_m = 2725$	$\Lambda'_m = 125$

#### IV. ENERGY LOSSES ASSOCIATED WITH GAPPED SCASA TRANSFORMER

SCASA coupled inductor shows transformer action only during transient propagation due its micro-henry order inductive coils [17]. Under 230 V/50 Hz AC operation, the two coils do not induce sufficient voltages to impede RMS current flow to the load. Therefore, in transient mode, when surge induced magnetic flux circulates through the SCASA core, coupled inductor stores a significant share of an incoming surge. The key motivation of using air-gapped ferrites is to increase the leakage of surge-induced flux and to intensify fringing flux eddy losses around the air gap. These core losses and elevated leakage levels are useful in optimizing SCASA surge suppression. In this Section, leakage and fringing effects of a gapped toroid and EER core will be investigated.

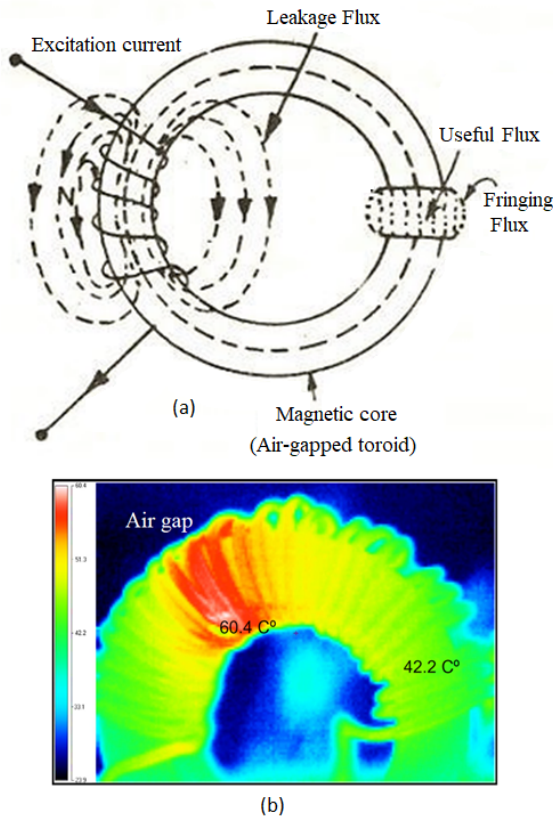


Fig. 6. Leakage and fringing flux associated with an air-gapped toroid: (a) flux lines distribution; (b) thermal image of a toroidal inductor [19]

##### A. Leakage Flux

Leakage flux is part of magnetic flux which does not follow the particularly intended path in a magnetic circuit, thus it is not used for magnetization of the core [20]. As shown in Fig. 6, leakage flux field in a toroid can appear across the core diameter as well as outside. Moreover, in cases where magnetic reluctance dominates, part of the flux that gets stored inside the relative components such as air-gaps also corresponds to leakage. From the initial investigation of leakage inductance measurements of gapped cores as per Table III, it was hard to obtain a clear pattern to explain the changes

of leakage flux in gapped core SCASA prototypes. Therefore, a percentage analysis based on the leakage percentages of primary and secondary windings wound to gapped-toroids was carried. Eq. 16 indicates how leakage percentages for both SCASA windings were evaluated.

$$\text{Leakage percentage} = \frac{\text{Leakage inductance}}{\text{Self inductance}} \times 100\% \quad (16)$$

Table III reveals consistent leakage percentages for the primary and secondary windings. In both cases, similarities are seen. According to Table III, it is clear that the ungapped toroid has almost zero leakage percentage, supporting a strong magnetic coupling between the two coils. Despite that, as pure ferrite core shows poor energy storage capability, primary and secondary coils fail to store much of the surge energy passing to the load. With the insertion of air-gaps, leakage flux levels are elevated, and this is validated by the test measurements of both primary and secondary windings showing significant leakage inductances. Accordingly, the double-gapped core was the most dominant with about 65–70% leakage percentages in both coils compared to 30–35% shown by the single-gapped core. As validated by LCR meter measurements illustrated by Fig. 8, these leakage trends remained steady for a 3–15 kHz frequency range. More information about leakage levels of powdered-iron toroid and air-gapped EER core is given in Table IV.

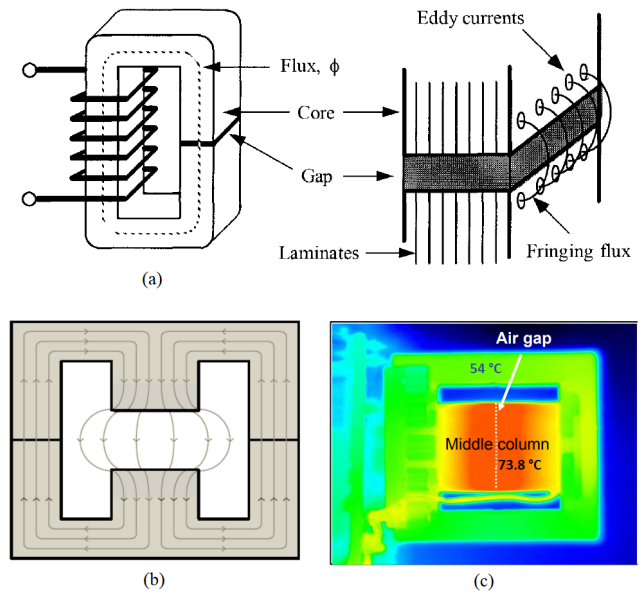


Fig. 7. Fringing flux associated with an air-gapped E-shaped ferrite: (a) excessive eddy current formation [13]; (b) fringing effect of EER gapped core (R43521A125); (c) thermal image of centre gapped ferrite [19]

##### B. Fringing Flux

The magnetizing flux when passes through the the air gap of a core, tends to bulge outward at as shown in Figs. 6 and 7. Due to this bulging effect, the effective cross-section of the air gap increases, and the flux density of the air gap decreases. This phenomenon is known as Fringing, and it is proportional to the length of the air gap. Thus, a significant fringing loss

is created with relatively larger air-gaps as depicted by Fig. 7(b).

Notably, the fringing flux lines when intersects the copper windings, can create excessive eddy current losses in the core windings as illustrated by Fig. 7(a). Though eddy-current losses of SCASA core due to fringing flux were not evaluated in this research, Figs. 6(b) and 7(c) found in [19] demonstrate how significant the corresponding heat dissipation can be for gapped core transformers. Following calculation approximates the energy loss due to fringing effect of EER gapped core:

According to [13], energy  $E_F$  stored in the fringing volume (extra volume due to bulging of field lines) around an air gap is given by;

$$E_F = E_o(F - 1) \quad (17)$$

where  $E_o$  is the energy stored purely in the air as per (9), and  $F$  is the fringing factor. For EER core  $F$  was calculated as 1.78. Substituting into (9) and (17),  $V_g = 200 \text{ mm}^3$  is the volume of air gap, and  $B_{max}=12.5 \text{ T}$  is the peak magnetic flux density across the core under a 3 kA transient;

$$E_o = 12.4 \text{ J} \rightarrow \text{Thus, } E_F = 9.7 \text{ J}$$

In this sense, it is possible to consider that extra energy (9.7 J) stored in the fringing volume is getting dissipated as eddy-current losses in the copper windings. A detailed

discussion about fringing field losses is beyond the scope of this paper.




According to the above discussion regarding leakage and fringing effects, it is evident that air-gapped transformers do possess significant energy losses. Thus, both leakage and fringing fields are positive aspects in surge protection circuits. The key idea is to leak and dissipate the surge-related magnetic flux during immediate propagation of a transient. To justify this discussion, inductance properties of SCASA coupled inductors designed using various gapped core configurations will be presented in the next Section.

## V. MEASUREMENT OF SELF- AND LEAKAGE INDUCTANCES OF SCASA TRANSFORMER

Using open- and short-circuit tests [21], self-inductances  $L_p$ ,  $L_s$  and leakage-inductances  $l_1$ ,  $l_2$  of SCASA prototype transformers (wound to ungapped, single-gapped, and double-gapped ferrite cores) were measured and compared with original Kool  $\mu$ u core. All the toroidal configurations tested for SCASA designs comprised of a coupled inductor (primary and secondary) wound at unequal number of turns. As in the original topology, primary winding has 6 turns, whereas secondary composed of 28 turns. Inductance measurements of both windings were carried out using a LCR meter (Fluke PM6304) at 10 kHz as summarized by Table III. The significance of air-gapping is demonstrated by the

TABLE III



COMPARISON OF MUTUAL, LEAKAGE AND SELF INDUCTANCES OF PRIMARY AND SECONDARY WINDINGS OF AIR-GAPPED CORES USED IN SCASA PROTOTYPE DESIGN

Measurement	Un-gapped Ferrite (ZW43615TC)	Single-gapped ferrite	Double-gapped ferrite
			
$L_p$ ( $\mu\text{H}$ )	312	13	6
$L_s$ ( $\mu\text{H}$ )	11,200	170	65
$N_1$	6	6	6
$N_2$	28	28	28
$l_1$ ( $\mu\text{H}$ )	2 (-0%)	4 (-30%)	4 (-67%)
$l_2$ ( $\mu\text{H}$ )	78 (-0%)	58 (-34%)	45 (-69%)
$M$ ( $\mu\text{H}$ )	1870	42	12
$k$	0.995	0.82	0.585

$L_p$ : primary self-inductance,  $L_s$ : secondary self-inductance,  $l_1$ : primary leakage-inductance,  $l_2$ : secondary leakage-inductance,  $M$ : mutual inductance,  $k$ : coupling coefficient,  $N_1$ : primary turns,  $N_2$ : secondary turns

TABLE IV

COMPARISON OF MUTUAL, LEAKAGE AND SELF INDUCTANCES OF PRIMARY AND SECONDARY WINDINGS FOR KOOL  $\mu$ U POWDERED-IRON TOROID (0077071A7) AND AIR-GAPPED FERRITE EER CORE (R43521A125) USED IN SCASA PROTOTYPE DESIGN

Measurement	Kool $\mu$ u Toroid (0077071A7) $\mu_r = 60$	Air-gapped EER core (R43521A125) $\mu_r = 105$
		
$L_p$ ( $\mu\text{H}$ )	3.4	7.7
$L_s$ ( $\mu\text{H}$ )	57	236.8
$N_1$	6	5
$N_2$	28	34
$l_1$ ( $\mu\text{H}$ )	1.6 (-47%)	3.6 (-46.7%)
$l_2$ ( $\mu\text{H}$ )	34.6 (-60%)	115.6 (-49%)
$M$ ( $\mu\text{H}$ )	9.8	31.5
$k$	0.74	0.74

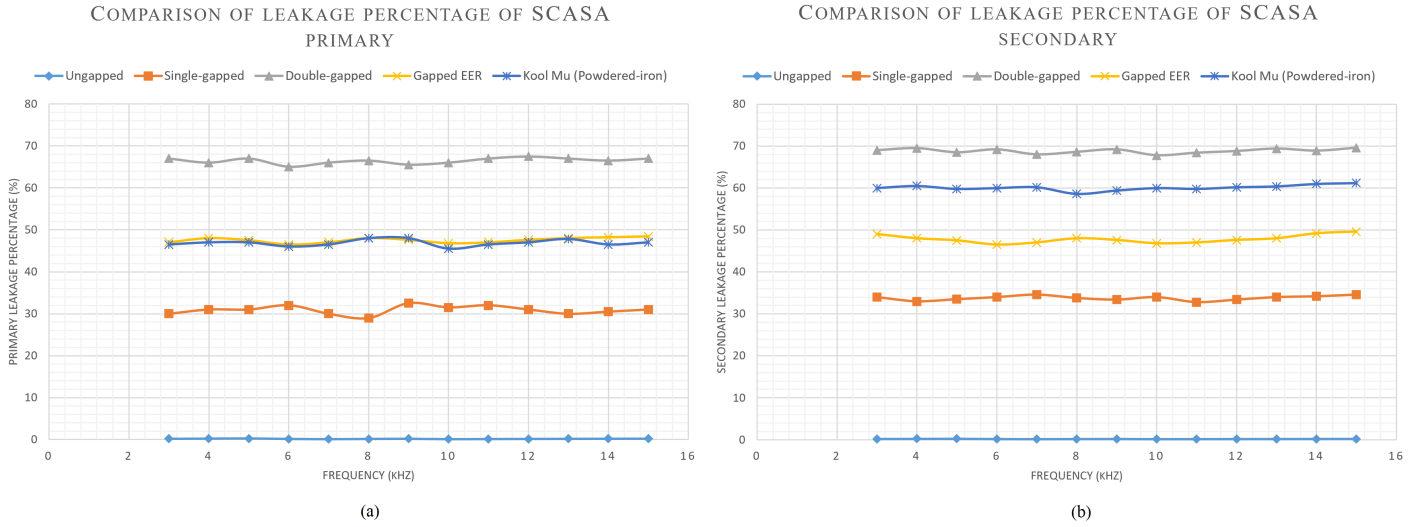


Fig. 8. Comparison of leakage percentages (from 3 kHz to 15 kHz) of SCASA coupled windings for the different core types under test: (a) Leakage percentage analysis of primary winding; (b) Leakage percentage analysis of secondary winding

variation of coupling coefficient  $k$  among three toroids as double-gapped core had the weakest magnetic coupling with  $k = 0.58$ , whereas ungapped core yielded  $k = 0.99$  with strong magnetic coupling and low leakage effects. This is further reflected by the notable drop in mutual inductance  $M$  among two gapped configurations compared to the pure ferrite which had  $M = 1870 \mu\text{H}$ . A discussion about the impact of leakage flux in gapped toroids is given below based on a leakage percentage analysis of SCASA primary and secondary (Fig. 8). As explained in Section IV, these lossy characteristics validated by inductance measurements associated with air-gapped toroids are useful in SCASA design. Next, self- and leakage inductance measurements of a SCASA surge protector prototype constructed using air-gapped ferrite EER (R43521A125) is presented.

#### A. Inductance properties of air-gapped EER core

Compared to the original SCASA transformer which utilized Kool  $\mu$  powdered-iron core, primary coil wound to the EER core has 5 turns, whereas the secondary composed of 34 turns. Inductance measurements of both coupled-inductor windings were carried out using a LCR meter (Fluke PM6304) at 10 kHz. Table IV presents essential inductance measurements taken for air-gapped EER core (R43521A125) with comparisons to Kool  $\mu$  powdered-iron core (0077071A7). More information about the energy storage capability of these core samples is provided in the following explanation.

According to Table IV, it is identifiable that both primary and secondary self-inductances ( $L_p$  and  $L_s$ ) are relatively higher in EER core compared to that of Kool  $\mu$  powdered-iron toroid. This is due to the comparatively high magnetizing permeance (inductance per turns squared) of EER core ( $\Lambda'_m = 125 \text{ nH/turn}^2$ ) in contrast to  $\Lambda_m = 61 \text{ nH/turn}^2$  of Kool  $\mu$  core. Since both coils possess  $\mu\text{H}$  level self-inductances, they do not impede 230 V mains flow under 50 Hz for this new EER configuration. As primary and secondary turns do not vary considerably for the two designs, the key concern is the alter-

ation of leakage inductances. The gapped EER based coupled inductor showed significant increases in leakage components with  $l_1 = 3.6 \mu\text{H}$  and  $l_2 = 115.6 \mu\text{H}$  for the respective coils compared to  $l_1 = 1.6 \mu\text{H}$  and  $l_2 = 34.6 \mu\text{H}$  of powdered-iron core. As per the percentage analysis of leakage effect described above (Leakage percentage =  $\frac{\text{Leakage inductance}}{\text{Self inductance}} \times 100\%$ ), 47% and 46.7% of leakage can be evaluated for primary coil of Kool  $\mu$  and EER cores respectively (see Fig. 8(a)). Interestingly, both core types possessed similar leakage percentages for the primary. But, the secondary winding yielded different leakage effects for the two designs with  $\sim 60\%$  and  $\sim 50\%$  respectively (see Fig. 8(b)).

The most noticeable comparison in Table IV is the variation magnetic coupling ( $k$ ) between the cores. Both powdered-iron and air-gapped EER cores showed a remarkable similarity in magnetic coupling with a coupling coefficient  $k = 0.74$  for the two prototypes. Therefore, it can be predicted that the minimum leakage flux should be  $\sim 26\%$  of the total flux, whereas 74% is coupled as useful flux. For a single surge pulse of 3 kA (8/20  $\mu\text{s}$  current wave, IEEE-C62.41) passing through SCASA coupled-inductor, it can be calculated that the maximum flux density  $\vec{B}_{max} = 12.5 \text{ T}$  [17]. Thus, maximum flux  $\phi_{max} = 1250 \mu\text{Wb}$  (for a cross-section of 100  $\text{mm}^2$ ), and suitable leakage flux  $\phi_{leakage} = 325 \mu\text{Wb}$  (at least  $\sim 26\%$  of the total flux). Based on the above observations, it is possible to infer that the relatively low-priced commercially available gapped EER core is ideally suited for SCASA surge suppression. With the aim of verifying the surge absorption capability, a SCASA prototype (see Fig. 9(c)) using air-gapped EER (R43521A125) is constructed; a performance comparison based on surge immunity tests is presented next.

## VI. CIRCUIT OPTIMIZATION USING SCASA PROTOTYPES

Reducing load-side voltage clamping, and advancing the surge endurance capacity of SCASA surge protector were the two main goals of using this new core configuration. In



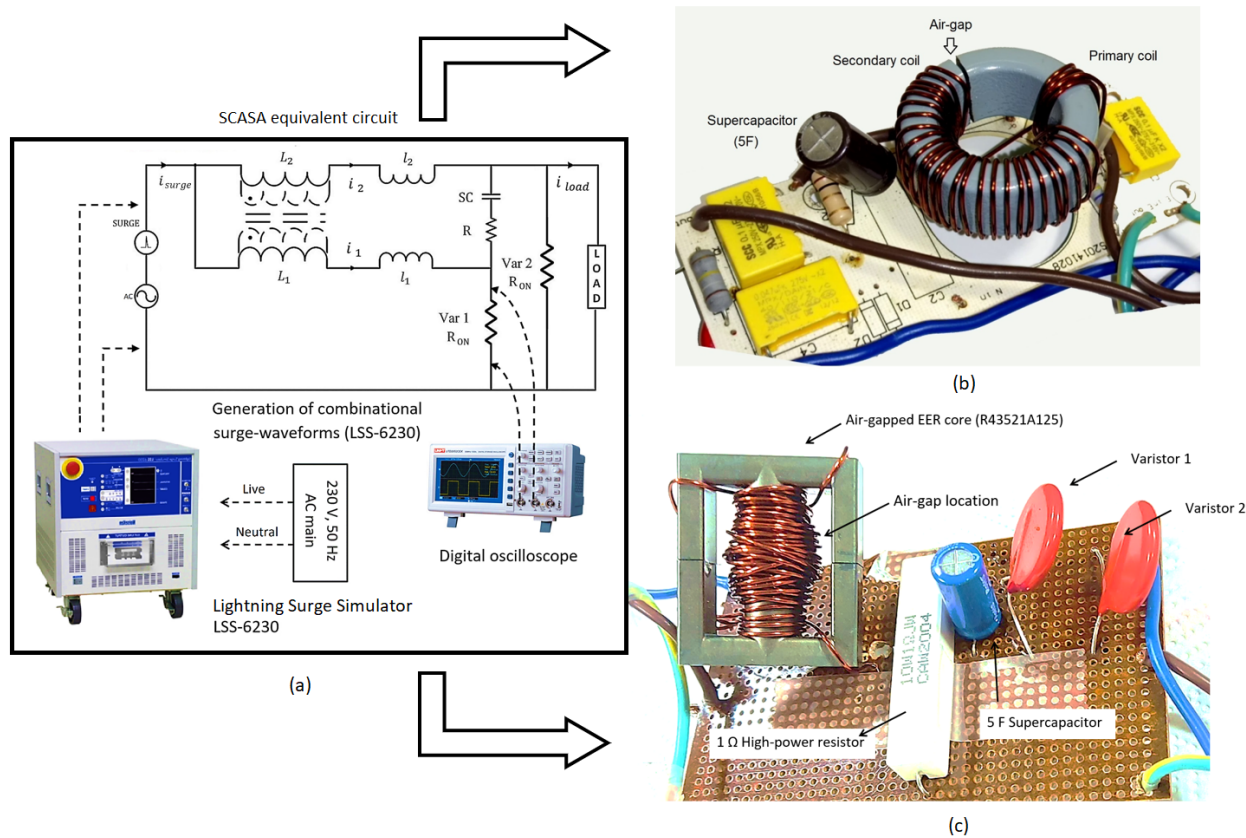


Fig. 9. Surge testing of SCASA prototypes: (a) schematic diagram of the measurement system [21]; (b) prototype using air-gapped toroid; (c) prototype using air-gapped EER core

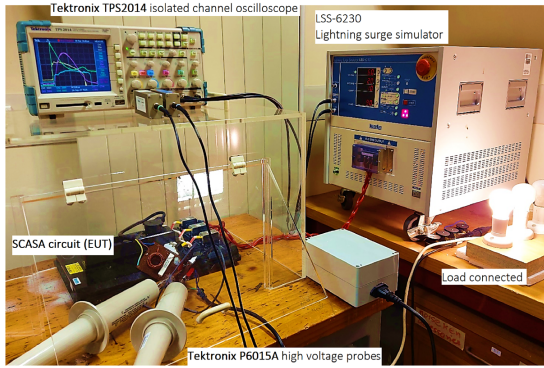
this section, suitability of EER type magnetic-core is explored by comparing its performance under transient operation. The SCASA prototype designed using gapped EER core (Fig. 9(c)) was subjected to standard combinational transients (1.2/50  $\mu$ s voltage wave, 8/20  $\mu$ s current wave as per IEEE-C62.41) to evaluate the surge endurance. In order to facilitate surge generation, a lightning surge simulator (LSS) NoisenKen-6230, high voltage probes (Tektronix P6015A) and an isolated-channel digital oscilloscope (Tektronix TPS2014) were used as the main instruments. Fig. 9(a) and 10(a) depict the schematic view and experimental setup implemented for 6 kV/3 kA combinational surge-waveform generation. Using UL-1449 3rd edition test procedures [22], oscilloscope waveforms were recorded for LSS peak settings across Varistor-1 and Varistor-2 of SCASA prototypes. Table V and Fig. 10 demonstrate the clamping voltage improvements of varistor-2 with comparisons made to original (Kool  $\mu$ u powdered-iron core) SCASA design.

#### A. Performance comparison: powdered-iron core vs air-gapped EER core

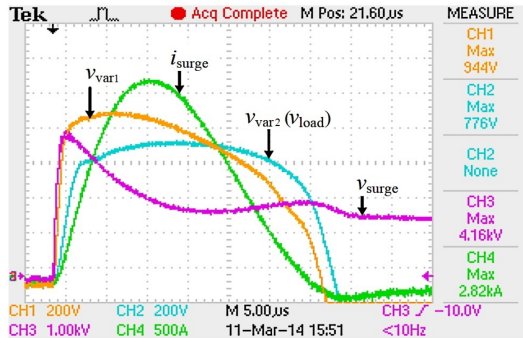
According to 10(b) and 10(c), both SCASA prototypes were subjected to approximately  $\sim 2.8$  kA maximum surge current. Out of the two SCASA varistors shown in 9(a), varistor-2 is of greater concern for this analysis as it is directly connected to the load-end. Noticeably, the SCASA prototype designed using gapped EER core showed an encouraging clamping voltage of 704 V for varistor-2 which is  $\sim 25$  % reduction

compared to the varistor-1. Conversely, the present SCASA design built using powdered-iron core recorded  $\sim 17$  % drop for the varistor-2 with 776 V clamping. Given the reduced varistor-2 voltage in EER based prototype, it is possible to infer that EER design is superior to the present topology in terms of surge absorption. More importantly, reduction percentage of varistor-2 clamping can be quantified as  $\sim 10$  % (Table V) which is a considerable improvement shown by the air-gapped prototype relative to present SCASA design.

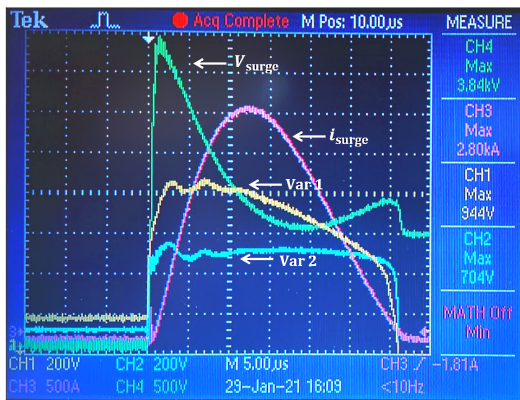
Another important aspect of gapped EER core is the energy losses associated with air-gap as described in Section IV: specially under transient operation when SCASA transformer becomes active, leakage flux and fringing losses can be significant. This gap effect drastically increase the total heat losses around the air gap (as described in Section IV). The fringing flux in EER core intersects the copper windings, creating excessive eddy currents in the SCASA coupled-inductor core. These unrestrained core losses facilitate the dissipation of surge energy and optimize the load-end voltage characteristics as indicated by Table V and Fig. 10. Furthermore, gapped ferrite cores have advantages over powder cores in terms of the manufacturing cost. With regard to the relatively easy production, gapped ferrites cost  $\sim 40$  % less compared to the complex manufacturing (air-bubble distribution) process of powdered-iron cores. The convenience of air-gap insertion in terms of trimming make these EER cores commercially affordable and mass-producible. Considering aforementioned factors, it is evident that air-gapped ferrite EER core (R43521A125) results



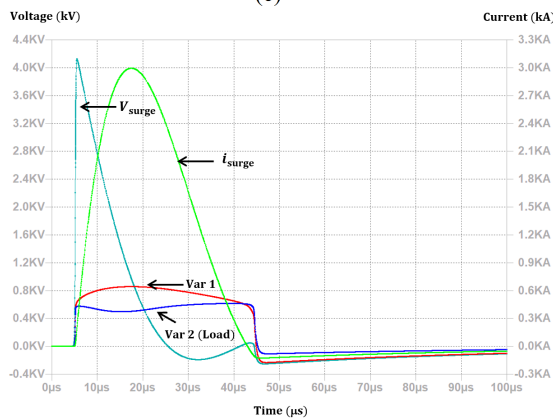
(a)



(b)



(c)



(d)

Fig. 10. Experimental setup and oscilloscope waveforms for different magnetic cores under a transient of 6 kV/3 kA: (a) experimental setup; (b) oscillogram for Kool  $\mu$ U powdered-iron core used in present SCASA design; (c) oscillogram for air-gapped EER ferrite core; (d) LTSpice simulated waveforms for gapped EER core

in a significant performance enhancement for SCASA surge suppression with a relatively low cost.

TABLE V  
COMPARISON OF CLAMPING LEVEL REDUCTION BY DIFFERENT SCASA PROTOTYPES BASED ON COMMERCIAL MAGNETIC CORES: KOOL  $\mu$ U POWDERED-IRON CORE (0077071A7) AND AIR-GAPPED FERRITE EER CORE (R43521A125)

Magnetic Core	Clamping voltage of Varistor 1 (V)	Clamping voltage of Varistor 2 (V)	Reduction percentage of Varistor 2 voltage
Kool $\mu$ U Powdered-iron Toroid (0077071A7)	944	776	$\sim 17\%$
Air-gapped EER core (R43521A125)	944	704	$\sim 25\%$

$$\text{Reduction percentage} = \frac{(776 - 704) \times 100}{776} = \sim 10\%$$

## VII. CONCLUSION

This study revealed that both leakage magnetic flux and fringing flux associated with air-gapped ferrites are useful for surge protector circuit design. Based on the research carried out using SCASA circuit prototypes, it was found that mass produced commercially available air-gapped EER core yields remarkable performance with  $\sim 10\%$  lower voltage clamping and better surge endurance than the Kool  $\mu$ U powdered-iron toroid. Notably, the two magnetic core designs showed an optimum magnetic coupling coefficient of  $k = 0.74$ . The analytical approach adopted based on permeance theory further revealed that the ideal effective-permeance range for gapped transformers is within  $67 < \Lambda_m < 125 \text{ nH/Turn}^2$ . This paper further includes self- and leakage inductance measurements for various SCASA designs, and confirm the validity of permeance model predictions using standard IEEE-C62.41 combinational surge waveforms injected to test prototypes. Experimental work for surge testing was carried out using a lightning surge simulator coupled with 230 V AC mains. In future research work, a frequency domain analysis of SCASA coupled-inductor will be carried out to predict the transient propagation through core windings.

## REFERENCES

- [1] IRDS 2020, 'The International Roadmap for Devices and Systems (IRDS): Beyond CMOS', (European Semiconductor Industry Association, Institute of Electrical and Electronics Engineers (IEEE), 2020), Technical report.
- [2] M.A. Laughton and D.F. Warne, Electrical Engineer's Reference Book, Elsevier Science, 2002.
- [3] IEC 60038:2009, 'IEC Standard Voltages'; International Electrotechnical Commission: Geneva, Switzerland, 2009-2020.
- [4] J.R. Barnes (Ed.), Transient Suppressors and Surge Suppressors. In Robust Electronic Design Reference Book; Springer: Berlin/Heidelberg, Germany, 2019.
- [5] R. B. Standler, Protection of Electronic Circuits from Overvoltages, Dover Books on Electrical Engineering, Courier Corporation, 2018.
- [6] N. Kularatna, J. Fernando, A. Pandey and S. James, Surge Capability Testing of Supercapacitor Families Using a Lightning Surge Simulator, in IEEE Transactions on Industrial Electronics, vol. 58, no. 10, pp. 4942-4949, Oct. 2011.

- [7] V. Chabot, J. Zhang, A. Yu, *Electrochemical Supercapacitors for Energy Storage and Delivery: Fundamentals and Applications*, United States: CRC Press, 2017.
- [8] 'Thor Technologies - STViQ/3 SMART TViQ', 2018. [Online]. Available at: <https://www.thortechnologies.com.au/product/stviq3/>, [Accessed: 22- April- 2021].
- [9] Magnetics Inc., '2020 Magnetics Powder Core Catalogue', Mag-inc.com. 2020. Available online: <https://www.mag-inc.com/Design/Technical-Documents/Powder-Core-Documents> [Accessed: 26- January- 2021].
- [10] N. Kularatna, A. Steyn-Ross, J. Fernando and S. James, *Design of Transient Protection systems: Including Supercapacitor Based Design Approaches for Surge Protectors*, Elsevier, USA, 2018, 284 pages.
- [11] S. T. Sadeeshvara Udayanga, N. Kularatna and D. A. Steyn-Ross, "Permeance based model for the coupled-inductor utilized in the supercapacitor assisted surge absorber (SCASA) and its experimental validation", 2nd IEEE International Conference on Industrial Electronics for Sustainable Energy Systems (IESES), Cagliari, Italy, 2020, pp. 267-272.
- [12] A. Bossche and V. Valchev, *Inductors and transformers for power electronics*. New York: Taylor & Francis, 2018.
- [13] C. McLyman, *Transformer and inductor design handbook*. New York: Marcel Dekker, 2004.
- [14] 'Air gapped magnetic cores', Surrey.ac.uk, 2011. [Online]. Available: <http://info.ee.surrey.ac.uk/Workshop/advice/coils/gap/index.html>. [Accessed: 04- Jan- 2019].
- [15] M. K. Kazimierczuk, *High-Frequency Magnetic Components*. Germany: Wiley, 2011.
- [16] Magnetics - 'Ferrite Core Documents', Mag-inc.com, 2017. [Online]. Available: <https://www.mag-inc.com/Design/TechnicalDocuments/Ferrite-Core-Documents>. [Accessed: 10- Dec-2020].
- [17] S. U. Silva Thotabaddadurage, *Permeance based Modelling, Design and Optimization of Supercapacitor Assisted Surge Absorber (SCASA) (Thesis, Doctor of Philosophy (PhD))*, 2021. The University of Waikato, Hamilton, New Zealand. Retrieved from <https://hdl.handle.net/10289/14602>.
- [18] Magnetics - 'Powder Core and Gapped Ferrite Core Comparison', Mag-inc.com, 2020. [Online]. Available: <https://www.mag-inc.com/Products/Powder-Cores/Learn-More-about-Powder-Cores/Gapped-Ferrite-Comparison>. [Accessed: 10- Nov-2020].
- [19] R. Kasikowski and B. Wiecek. Ascertainment of fringing-effect losses in ferrite inductors with an air gap by thermal compact modelling and thermographic measurements. *Applied Thermal Engineering*, 124:1447-1456, 2017.
- [20] H. Büilent Ertan, J. Turowski, X. M. López-Fernández, *Transformers: Analysis, Design, and Measurement*. (2017). United States: CRC Press.
- [21] S. T. Sadeeshvara Udayanga, S. Kokuhennadige, J. Fernando, N. Kularatna and D. A. Steyn-Ross, "Supercapacitor assisted surge absorber (SCASA) technique: selection of magnetic components based on permeance", 36th IEEE Applied Power Electronics Conference and Exposition (APEC), Arizona, USA, 2021, pp. 2299-2304.
- [22] UL 1449, 'UL Standard for Surge Protective Devices', 5th ed.; Underwriters Laboratories Inc.: Brooklyn, IL, USA, 2021.



**Sadeeshvara Silva** (S'18-M'20) was born in Colombo, Sri Lanka. He holds a Ph.D. in Electronic Engineering from the University of Waikato, New Zealand (2021) and a B.Sc. (Hons.-1st class) from University of Sri Jayewardenepura, Sri Lanka (2014).

Soon after his doctoral study, he joined Electric Power Engineering Centre, University of Canterbury as a Research Engineer in 2022. Prior to joining EPE Centre, he was involved as an academic researcher with the University of Waikato. During his time in Sri Lanka, he worked for University of Kelaniya and University of Sri Jayewardenepura.

Dr. Sadeeshvara Silva acts as a reviewer for IEEE Transactions on Industrial Electronics, IEEE Transactions on Power Electronics, IET Power Electronics and for IEEE conferences such as APEC, IECON, and TENCON. He is also a Member of Engineering NZ, IEEE, IET, SLAAS and RASSL. He won the IEEE Young Professionals Award (SYPA) at the 28th ISIE conference in Canada, 2019. He is passionate in research on power quality & surge protection, supercapacitor applications, transformer theory & design, EV charging technologies and magnetics.



**Nihal Kularatna** (SM-98) is research-active in supercapacitor applications and power electronics. He has authored ten reference books and research monographs, and contributed over 170 publications. He won the Post Graduate Research Supervision Excellence Award (2021) from the University of Waikato where he is employed as an associate professor. For developing supercapacitor assisted (SCA) techniques he won the NZ Engineering Innovator of the Year 2013 award. He was conferred a DSc degree in

2015. Prior to moving to academia in New Zealand, he was the CEO of Arthur C Clarke Institute in Sri Lanka.



**D. Alistair Steyn-Ross** earned his BSc (1975), MSc (hons, 1977), and PhD (2002) degrees in Physics at the University of Waikato (UoW), New Zealand. He is an associate professor with the School of Engineering, UoW. His research expertise is the application of computational physics and mathematics to modelling of non-linear stochastic systems during close approach to phase transition critical points. He has supervised a substantial number of PhD projects in the application of supercapacitors to renewable-

energy storage and the design of robust, energy-efficient DC power supplies, and has co-authored over 25 papers on supercapacitor-related topics.